Title

Multispectral SWIR images of the pulp-chamber of posterior teeth in vitro

Permalink

https://escholarship.org/uc/item/5731h38d

Authors

Simon, Jacob C
Mogire, Emmanuel O
Yun, Sam Y
et al.

Publication Date

2021-03-01

DOI

10.1117/12.2584900

Peer reviewed

Multispectral SWIR images of the pulp-chamber of posterior teeth *in vitro*

Jacob C. Simon, **Emmanuel O. Mogire**, **Sam Y. Yun**, **Daniel Fried**

University of California, San Francisco, San Francisco, Ca 94143-0758

Abstract

Intraoral imaging of teeth with SWIR light provides increased contrast of dental caries and restorative materials compared to visible inspection and digital radiography. The objective of this study was to investigate the SWIR optical properties of the dental pulp-chamber floor, walls and canal orifices. We imaged *in vitro* extracted human posterior teeth at 1300-nm and 1500–1700-nm in reflectance and transillumination and compared the tissues properties with visible light images and quantitative light fluorescence. Transillumination of posterior teeth at both 1300-nm and 1500–1700-nm yielded significantly higher contrast between the pulp-chamber floor and walls than all other methods tested.

Keywords

SWIR imaging; detection; reflectance; transillumination; endodontics; root canal

1. INTRODUCTION

Non-surgical root canal therapy (RCT) is prescribed by general dentists and endodontists when the dental pulp becomes infected (pulpitis), irreversibly inflamed and/or necrotic to save the tooth and guard the supporting bone or adjunct anatomy from the spread of infection. The most common etiologies of pulpitis are dental decay, trauma, repeated dental procedures performed on the tooth, faulty crowns, crown-originating dental fractures (cracks) that provide a route for bacteria to infect the endodontic soft tissue or overheating the tooth causing pulpal cell death. A successful non-surgical root canal treatment is assessed in four dimensions, with the first encompassing acute pain relief by controlled reduction of infection and inflammation [1]. The procedure consists of the removal of the source responsible for the endodontic diagnosis followed by adequate pulp-chamber access, chemo-mechanical cleaning and shaping of the radicular canal system, canal obturation and a final restoration sealing the endodontic system from the oral cavity. While the reported mean success rate (complete healing) for primary RCT is 83% (95% CI:0.77–0.89) when vital pulpectomy is performed and 72% (95% CI:0.67–0.78) when established lesions are present, advances are desired to improve treatment outcomes [2–6]. A major treatment related cause in why endodontically treated teeth fail is inadequate chemo-mechanical instrumentation of the root-canal system and missed canals. Amongst the most common missed canals associated with persistent periapical disease are the second canal of the maxillary molars (MB2 canal), lingual canals of mandibular incisors and premolars, and the middle mesial and distolingual canals of mandibular molars [7, 8].

In 2004, Krasner and Rankow published *Anatomy of the Pulp-Chamber Floor* that provided a statistics based set of *laws* pertaining to the relationships between the pulp chamber and clinical crown and the pulp-chamber floor [9]. The final law proposed by Krasner and Rankow, the law of orifice location 3: stating that the orifices of the root canals are located at the terminus of the root developmental fusion lines, is the only law proposed that aids in determining the canal orifice position and number based on the precise morphology of the tooth in question [9]. The reason the law of orifice location 3 is distinctly valuable among the set is due to the fact that the pulp-chamber floor has a developmental origin independent from the Hertwig's epithelial root sheath (HERS) dental papilla interaction responsible for dentinogenesis of the roots [10]. In humans, the intraradicular dentin that eventually becomes the pulp-chamber floor develops from the subpupal lobe, a separate mineralization center that only later in growth unites with the coronal and root dentin [10–12]. The quantity of secondary lobes and their distribution determines the number of roots formed and the shape observed by the clinician formed by the subpulpal grooves [10]. The connecting lines among the subpulpal lobes on the completed tooth consists of a ridge on the external surface (interradicular crista), and a groove or isthmus on the internal surface (subpulpal groove) [11, 13]. Together these structures comprise the root development fusion lines what appear as a pulp chamber dark zone surrounding the entrances of the root canals and connecting with each other in common topologies [14, 15].

With direct observation of this anatomic element the endodontist can topographically follow the root development fusions lines using supplementary instruments such as operating microscopes. The use of the dental operating microscope (DOM) during endodontic procedures provides enhanced vision, magnification and illumination of the operative field producing more successful treatment outcomes. Dozens of studies demonstrate that the DOM improves identification and treatment of additional anatomy (less missed canals) and diagnosis of caries and cracks [16–21]. When equipped with a beam splitter, CCD cameras can be attached to the DOM to provide digitization of the clinicians' operative view, procedural documentation and the perform quantitative optical measurements. Most clinical microscopes have integrated digital capabilities, however very little has been done to leverage the data acquired through imaging for non-surgical and surgical root canals [22, 23].

Over the past decade short wavelength infrared (SWIR) imaging from 1300–1700-nm in reflectance and transillumination has demonstrated improved diagnostic performance for caries identification and crown-originating crack detection compared to visible/tactile methods and digital radiography [24–29]. Imaging with SWIR light benefits from a markedly reduced scattering coefficient and variable water absorption throughout the spectral window permitting deeper penetration of transilluminated or back scattered light and increased contrast of caries and cracks relative to sound tissue [28]. With these optical advantages and compatibility with the dental operative microscope, integration of SWIR imaging during the root canal treatment can be achieved without compromise by the clinician. Shemesh et al. [30, 31] investigated the use of optical coherence tomography at 1300-nm for endodontic imaging. However, there have not been any published investigations of the SWIR optical properties comprising the pulp-chamber anatomy.

The objective of this study was to investigate the SWIR optical properties of the tissues surrounding and forming the pulp-chamber floor, walls and canal orifices. We constructed a SWIR surgical microscope with the capability of 7x magnification and imaged *in vitro* extracted human posterior teeth at 1300-nm and 1500–1700-nm in reflectance and transillumination and compared the tissues properties with visible light images and quantitative light fluorescence.

2. MATERIALS and METHODS

2.1 Sample Preparation

Posterior teeth (n=30) were selected with sound coronal structure and fully developed root systems for participation in this study. Teeth were collected from patients in the San Francisco Bay area with approval from the UCSF Committee on Human Research. The teeth were sterilized using gamma radiation and stored in 0.1% thymol solution to maintain tissue hydration and prevent bacterial growth. Samples were mounted in black orthodontic resin in order to facilitate repeatable imaging angle and orientation. Samples were decoronated 2–4-mm above the cementoenamel junction (CEJ) using a linear precision saw, Isomet 2000 (Buehler, Lake Buff, IL). A high-speed dental handpiece equipped with an Endo-Z bur was used to refine the endodontic access with straight line access. The intent for the sample preparation was to expose the pulp-chamber floor in the same manner as Krasner and Rankow [9]. The pulp-chambers were debrided of any organic material using hypochlorite and K-files with the desire not to enlarge or alter the canal orifices.

2.2 Visible Reflectance Images

A Dino-Lite digital microscope, Model 5MP Edge AM7915MZT, AnMO Electronics Corp. (New Taipei City, Taiwan) was used to acquired visible images of all samples. The digital microscope captures 5 mega-pixel (2,952 × 1,944) color images. Eight white LED lights contained in the camera illuminate the sample and a single polarization element is utilized to help reduce glare.

2.3 Visible Transillumination Images

Samples were illuminated in occlusal transillumination using a quadfurcated fiber optic bundle to deliver unpolarized light angled apically at the cementoenamel junction from both sides (buccal/lingual) of the tooth with a broadband tungsten halogen lamp (E Light, Denver, Colorado) [32]. Images were captured with a Sony α7RII digital camera with 42.4 mega pixel full frame sensor (ILCE-7RM2) equipped with a Sony FE 90-mm f/2.8 Macro G OSS lens (SEL90M28G).

2.4 Quantatative Light Fluorescence (QLF) Images

A Dino-Lite digital microscope, with 5 blue light-emitting diodes and a 510-nm LP filter, Model AM4115TW-GFBW from AnMO Electronics Corp. (New Taipei City, Taiwan), were used to acquire fluorescence images of the pulp chamber floor.

2.5 SWIR Occlusal Transillumination and Reflectance Imaging System

A high sensitivity, InGaAs SWIR camera, Model SU320KTSX from Sensors Unlimited (Princeton, NJ) with a 320×256-pixel focal plane array and 12.5-μm pixel pitch was used to capture SWIR reflectance and occlusal transillumination images of posterior teeth *in vitro* [32, 33]. The camera was equipped with a zoom lens Model 70XL from Zast Corporation (Seoul, South Korea) with a 7:1 magnification range. Sample images were illuminated with filtered light from two broadband tungsten halogen lamps from E Light (Denver, Colorado) delivered through separate reflectance and transillumination fiber optic cable bundles. Reflectance illumination was achieved using a ring light from Volpi (Auburn, NY). Occlusal transillumination used a quadfurcated fiber optic bundle to deliver unpolarized light angled apically at the cementoenamel junction from both sides (buccal/lingual) of the tooth. The output of the broadband light source was filtered with optical filters housed in a motorized filter wheel, FW102 from Thorlabs. The filter wheel contained long pass λ=1500-nm filter from Spectragon (Parsippany, NJ) and band pass λ=1300-nm from Thorlabs. The 12-bit image data was delivered over a camera link cable to a Real Time PXIe-1071 chassis with NI-8133 embedded controller and NI-1428 camera link image acquisition board from National Instruments (Austin TX).

2.6 Image analysis

All images were converted to 8-bit grey scale data types using built in algorithms in Labview. The contrast between the pulpal floor and walls was calculated using NI Vision Assistant, by hand selecting the region of interest and averaging the pixel intensity of the selected region. The average intensity value was used to calculate the lesion contrast with the formula $(I_w - I_F)/I_w$ where W=wall and F=floor. This formula normalizes the percent contrast from 0–1.

2.6 Statistical Analysis

Statistics were obtained using Prism from Graphpad software (San Diego, CA). Contrasts values were compared with near-IR measurements using repeated measures one-way analysis of variance (ANOVA) followed by Tukey-Kramer post-hoc multiple comparison test.

3. RESULTS and DISCUSSION

In this study we successfully designed and fabricated a dental operative microscope equipped with InGaAs camera sensor capable of capturing images at 7x magnification of the endodontic space in reflectance and transillumination from 1300–1700-nm. In the same manner as Krasner and Rankow we used sound extracted posterior teeth and decoronated the samples 2–4-mm above the CEJ to preserve the relationship between the pulp-chamber walls and floor and debrided any remaining soft tissue with hypochlorite. We imaged the exposed pulp-chambers with visible reflectance, SWIR reflectance at 1300-nm and 1500–1700-nm, QLF, visible transillumination and SWIR transillumination at 1300-nm and 1500–1700-nm (Fig. 1). Using image analysis software, we calculated the contrast of the features defining the pulp-chamber floor, most notably, the contrast of the developmental fusion lines which reveal the distribution of roots and canals in posterior teeth.

The mean contrast values ± standard deviation for the most remarkable reflectance wavelengths are presented in Fig. 2 and Table 1. Visible light and SWIR reflectance images showed the greatest contrast of the developmental fusion lines measuring 31.13% and 28.66% respectively and both were superior to QLF measuring 16.21%. There appears to be subtle shape and contour differences between the development fusion lines most likely attributed to the composition of the dentin in this region and the interaction of the imaging wavelength. This region is comprised of the distinct lays of dentin, with the apical layer adjacent to the cementum consisting of regularly arranged dentin tubules oriented 90-degree to the root surface. In the central area of the bifurcation the dentinal tubules frequently alter their direction multiple times and merge with the second zone that demonstrates complex three-dimensional decussation patterns [15, 34]. The zone closest to the pulp appears very dark with haphazard collagen deposition that is relatively radiolucent and hypomineralized. SWIR reflectance from 1500–1700-nm showed almost no contrast of the pulp-chamber floor due to the significant water absorption and greater optical penetration in that spectral region. It should be noted that despite this lack of contrast among that hard tissue comprising the pulp-chamber floor and walls, SWIR reflectance at wavelengths coincident with high water absorption may yield high contrast between the soft tissues in the chamber and canals prior to debridement and should be investigated further in experiments replicating *in vivo* conditions more accurately.

Visible and SWIR transillumination showed superior contrast than all reflectance imaging methods (Table 2). We hypothesize that this is due the light scattering through the exterior of the tooth into the furcation zone and attenuation by the disorganized dentin tubules from the interradicular crista and the subpulpal groove [35]. Visible transillumination performed better than expected demonstrating 37.26% contrast possibly due the lack of gingival tissue, cleanliness of the pulp-chamber that was well cleaned with hypochlorite and free of heme, and/or due to the quality of the illumination apparatus employed. Both SWIR transillumination at 1300-nm and 1500–1700-nm outperformed visible transillumination yielding extremely high contrast of the pulp-chamber floor anatomy with 50.35% and 64.34% contrast respectively. In addition to the high contrast, both SWIR modalities show small standard deviation values illustrating the ease and consistency that SWIR transillumination images can be executed in endodontic applications. Unlike visible light, the SWIR wavelengths utilized are beyond the absorption bands of hemoglobin and other biological tissues that could interfere with *in vivo* transillumination imaging clinically.

Observing the images in Figs. 1&2 it is obvious how well illuminated the pulp-chamber is in SWIR transillumination. The ability to see cracks in the SWIR was been demonstrated previously looking at the coronal surface, but investigation of crown-originating cracks that enter the pulpal floor from 1300–1700-nm deserves serious consideration in future studies.

This study illustrates the potential of SWIR reflectance and transillumination imaging for the improved identification of endodontic anatomy and could facilitate more complete endodontic treatment and better patient outcomes. Without any influential changes to the current operative environment, more informative optical data can be acquired of the treated tooth, leading to easier identification of all canal orifice through clear visualization of the pulp-chamber floor developmental fusion lines. Equipping DOMs with new imaging

technologies could result in faster, less stressful procedures and a greater in-operation understanding of the tooth's hard tissue structure which clinicians have never had access to. In addition to the solely endodontic motivations, the increased contrast of dental caries and cracks that we have previously show, adjunctively contribute to a more technology driven and unbiased way determine decay removal in cases that may be treated with less aggressive strategies such as vital tooth approaches or prevent unnecessary endodontic treatment if the tooth has a poor prognosis.

ACKNOWLEDGEMENTS

5. REFERENCES

[1]. Gulabivala K, and Ng Y-L, Outcomes of Endodontic Therapy PMPH USA, 33 (2019).

[2]. Torabinejad M, Corr R, Handysides R, and Shabahang S, "Outcomes of nonsurgical retreatment and endodontic surgery: a systematic review," J Endod, 35(7), 930–7 (2009). [PubMed: 19567310]

[3]. Gilbert GH, Tilashalski KR, Litaker MS, McNeal SF, Boykin MJ, Kessler AW, and Group DC, "Outcomes of root canal treatment in Dental Practice-Based Research Network practices," Gen Dent, 58(1), 28–36 (2010). [PubMed: 20129890]

[4]. Elemam RF, and Pretty I, "Comparison of the success rate of endodontic treatment and implant treatment," ISRN Dent, 2011, 640509 (2011). [PubMed: 21991484]

[5]. Ng YL, Mann V, Rahbaran S, Lewsey J, and Gulabivala K, "Outcome of primary root canal treatment: systematic review of the literature -- Part 2. Influence of clinical factors," Int Endod J, 41(1), 6–31 (2008). [PubMed: 17931388]

[6]. Ng YL, Mann V, Rahbaran S, Lewsey J, and Gulabivala K, "Outcome of primary root canal treatment: systematic review of the literature - part 1. Effects of study characteristics on probability of success," Int Endod J, 40(12), 921–39 (2007). [PubMed: 17931389]

[7]. Hiebert BM, Abramovitch K, Rice D, and Torabinejad M, "Prevalence of Second Mesiobuccal Canals in Maxillary First Molars Detected Using Cone-beam Computed Tomography, Direct Occlusal Access, and Coronal Plane Grinding," J Endod, 43(10), 1711–1715 (2017). [PubMed: 28735796]

[8]. Siqueira JF Jr., "Aetiology of root canal treatment failure: why well-treated teeth can fail," Int Endod J, 34(1), 1–10 (2001). [PubMed: 11307374]

[9]. Krasner P, and Rankow HJ, "Anatomy of the pulp-chamber floor," J Endod, 30(1), 5–16 (2004). [PubMed: 14760900]

[10]. Kondo S, and Hanamura H, "How Does the Pulpal Floor of a Molar Tooth Develop?," Journal of Oral Biosciences, 51(4), 205–209 (2009).

[11]. Jorgensen KD, "Macroscopic observations on the formation of the sub-pulpal wall," Odontol Tidskr, 58(2), 83–103 (1950). [PubMed: 14785898]

[12]. Ooe T, and Gohdo S, "The development of the human interradicular dentine as revealed by tetracycline-labelling," Arch Oral Biol, 29(4), 257–62 (1984). [PubMed: 6586122]

[13]. Everett FG, Jump EB, Holder TD, and Williams GC, "The intermediate bifurcational ridge: a study of the morphology of the bifurcation of the lower first molar," J Dent Res, 37(1), 162–9 (1958). [PubMed: 13513891]

[14]. Acosta Vigouroux SA, and Trugeda Bosaans SA, "Anatomy of the pulp chamber floor of the permanent maxillary first molar," J Endod, 4(7), 214–9 (1978). [PubMed: 283185]

[15]. Foreman PC, and Soames JV, "Analysis of the pulp chamber floor of human molar teeth," Int Endod J, 21(4), 257–63 (1988). [PubMed: 3251850]

[16]. Low JF, Dom TNM, and Baharin SA, "Magnification in endodontics: A review of its application and acceptance among dental practitioners," Eur J Dent, 12(4), 610–616 (2018). [PubMed: 30369811]

[17]. Forgie AH, Pine CM, and Pitts NB, "The use of magnification in a preventive approach to caries detection," Quintessence Int, 33(1), 13–6 (2002). [PubMed: 11887530]

[18]. Clark DJ, Sheets CG, and Paquette JM, "Definitive diagnosis of early enamel and dentin cracks based on microscopic evaluation," J Esthet Restor Dent, 15(7), 391–401; discussion 401 (2003). [PubMed: 15000906]

[19]. Mamoun JS, and Napoletano D, "Cracked tooth diagnosis and treatment: An alternative paradigm," Eur J Dent, 9(2), 293–303 (2015). [PubMed: 26038667]

[20]. de Carvalho MC, and Zuolo ML, "Orifice locating with a microscope," J Endod, 26(9), 532–4 (2000). [PubMed: 11199796]

[21]. Schwarze T, Baethge C, Stecher T, and Geurtsen W, "Identification of second canals in the mesiobuccal root of maxillary first and second molars using magnifying loupes or an operating microscope," Aust Endod J, 28(2), 57–60 (2002). [PubMed: 12360670]

[22]. Harrel SK, Abraham CM, Rivera-Hidalgo F, Shulman JD, and Nunn ME, "Videoscope-assisted minimally invasive periodontal surgery (V-MIS)," J Clin Periodontol, 41(9), 900–7 (2014). [PubMed: 25039580]

[23]. van As GA, "Digital documentation with the dental operating microscope," Pract Proced Aesthet Dent, 16(3), suppl 6–7 (2004).

[24]. Simon JC, Lucas SA, Lee RC, Staninec M, Tom H, Chan KH, Darling CL, and Fried D, "Near-IR Transillumination and Reflectance Imaging at 1300-nm and 1500–1700-nm for in vivo Caries Detection," Lasers Surg Med, 48(6), 828–836 (2016). [PubMed: 27389018]

[25]. Simon JC, Lucas SA, Staninec M, Tom H, Chan KH, Darling CL, and Fried D, "Transillumination and reflectance probes for near-IR imaging of dental caries," Lasers in Dentistry XX. Proc SPIE Vol. 8929: D1–7 (2014).

[26]. Simon JC, Chan KH, Darling CL, and Fried D, "Multispectral near-IR reflectance imaging of simulated early occlusal lesions: variation of lesion contrast with lesion depth and severity," Lasers Surg Med, 46(3), 203–15 (2014). [PubMed: 24375543]

[27]. Fried D, Buhler CM, Ngaotheppitak P, and Darling CL, "Near-IR imaging of interproximal lesions from occlusal surfaces and the influence of stains and plaque." Proc SPIE, Vol. 6137 N:1–7 (2006).

[28]. Darling CL, and Fried D, "Optical properties of natural caries lesions in dental enamel at 1310-nm," Lasers in Dentistry XI. Proc SPIE, Vol. 5687 34–41 (2005).

[29]. Fried WA, Simon JC, Lucas S, Chan KH, Darling CL, Staninec M, and Fried D, "Near-IR imaging of cracks in teeth," Lasers in Dentistry XX. Proc SPIE Vol. 8929 Q:1–6 (2014).

[30]. Shemesh H, van Soest G, Wu MK, van der Sluis LW, and Wesselink PR, "The ability of optical coherence tomography to characterize the root canal walls," J Endod, 33(11), 1369–73 (2007). [PubMed: 17963966]

[31]. Shemesh H, van Soest G, Wu MK, and Wesselink PR, "Diagnosis of vertical root fractures with optical coherence tomography," J Endod, 34(6), 739–42 (2008). [PubMed: 18498903]

[32]. Simon JC, Darling CL, and Fried D, "A system for simultaneous near-infrared reflectance and transillumination imaging of occlusal carious lesions," Lasers in Dentistry XXI. Proc. SPIE Vol. 9692: A1–6 (2016).

[33]. Simon JC, Darling CL, and Fried D, "Assessment of cavitation in artificial approximal dental lesions with near-IR imaging," Lasers in Dentistry XXIII. Proc. SPIE Vol. 10044 7:1–7 (2017).

[34]. Goldberg M, Kulkarni AB, Young M, and Boskey A, "Dentin: structure, composition and mineralization," Front Biosci (Elite Ed), 3, 711–35 (2011). [PubMed: 21196346]

[35]. Tidmarsh BG, "Micromorphology of pulp chambers in human molar teeth," Int Endod J, 13(2), 69–75 (1980). [PubMed: 6935174]
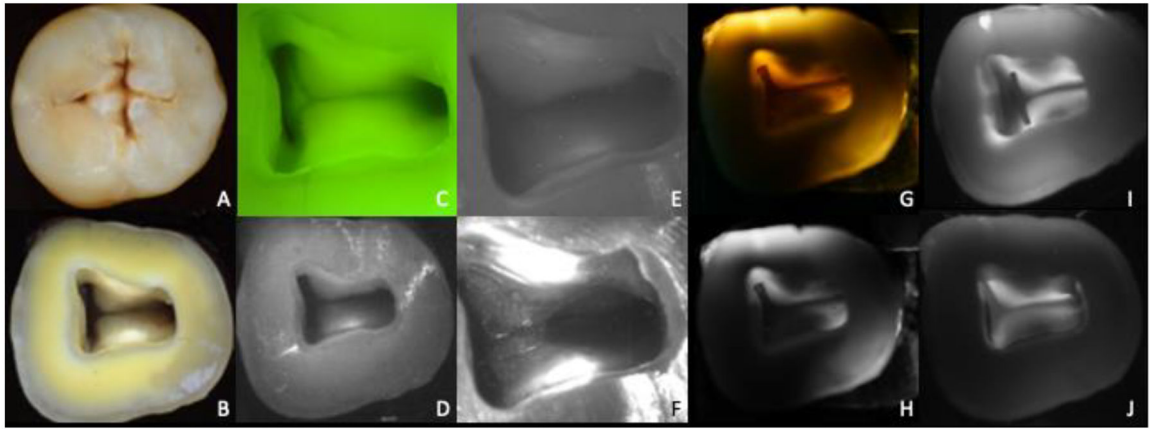
Fig. 1.
Reflectance and transillumination images of a mandibular molar, (A) visible reflectance before sample preparation, (B) visible reflectance, (C) QLF reflectance, (D) BP1300-nm reflectance, (E) BP-1300-nm reflectance, (F) LP1500-nm reflectance, (G) visible transillumination color, (H) visible transillumination greyscale, (I) BP1300-nm transillumination, and (J) LP1500-nm transillumination.
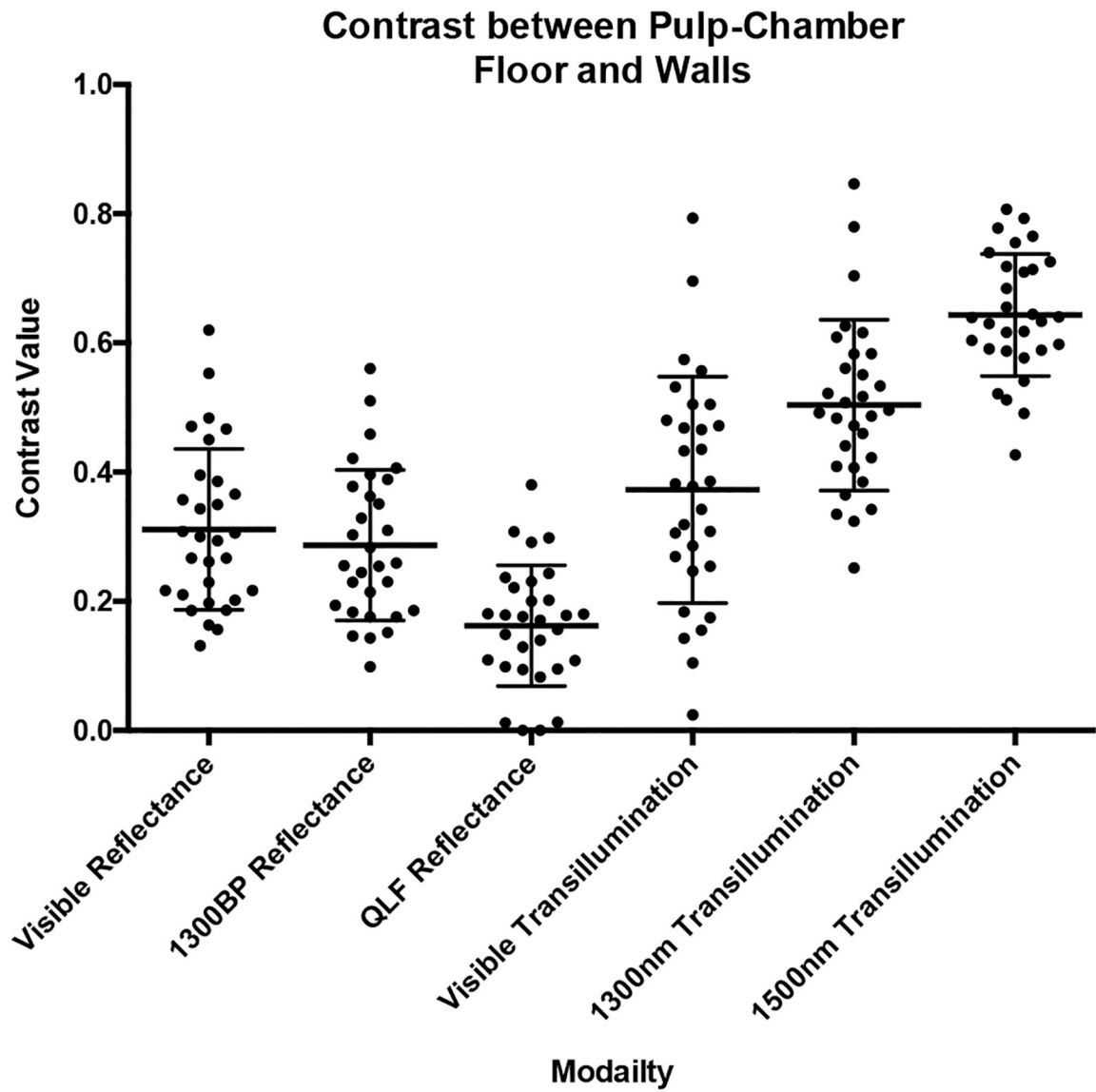
Fig. 2.
Contrast values for each modality and spectral region between the pulp-chamber floor and walls. SWIR wavelengths outperformed visible light producing greater contrast of pulp chamber anatomy.
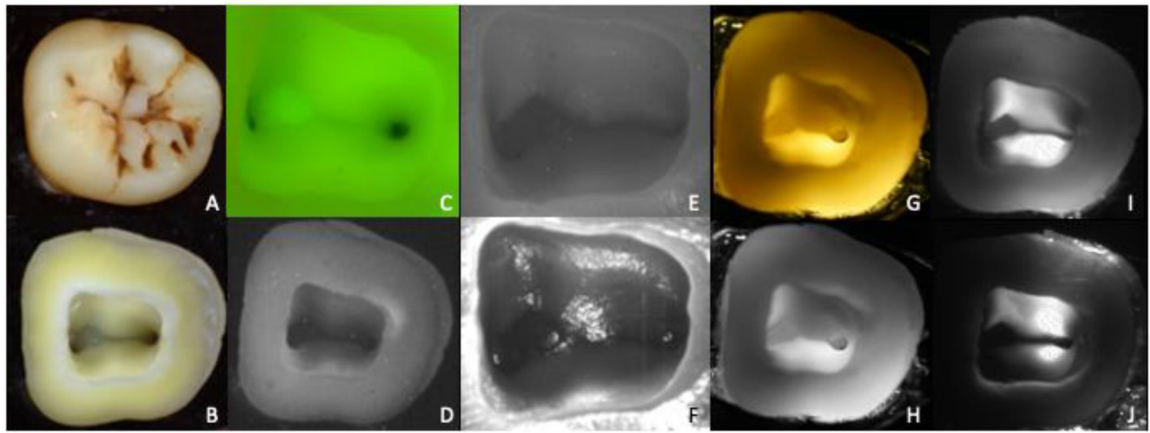
Fig. 3.
Reflectance and transillumination images of a mandibular second molar, (A) visible reflectance before sample preparation, (B) visible reflectance, (C) QLF reflectance, (D) BP1300-nm reflectance, (E) BP-1300-nm reflectance, (F) LP1500-nm reflectance, (G) visible transillumination color, (H) visible transillumination greyscale, (I) BP1300-nm transillumination, and (J) LP1500-nm transillumination.

Table 1.

Percent contrast values of reflectance images ± S.D. and statistical group. There was no detected difference between visible reflectance and SWIR reflectance at 1300-nm. Both visible and 1300-nm reflectance significantly outperformed QLF.

	Visible Ref.	1300-nm Ref.	QLF
% Contrast	31.13 ± 12.44	28.66 ± 11.65	16.21 ± 9.35
Statistical Group	a	a	b

Table 2.

Contrast values of transillumination images ± S.D. and statistical group. All groups are statically significant from each other. 1500-nm transillumination demonstrated the highest contrast.

	Visible Trans.	1300-nm Trans.	1500-nm Trans.
Contrast	37.26 ± 17.54	50.35 ± 13.24	64.34 ± 9.45
Statistical Group	a	b	c